Electronic Supplementary Material (ESI) for Materials Horizons.
This journal is © The Royal Society of Chemistry 2021

Supporting Information

Scalable Fluid-spinning Nanowire-based Inorganic Semiconductor Yarns for Electrochromic Actuators

Linpeng Li, Kun Wang, Hongwei Fan, Xiangyu Zhu, Jiuke Mu*, Hao Yu*, Qinghong Zhang, Yaogang Li, Chengyi Hou*, Hongzhi Wang

Experimental procedures

Materials. V_2O_5 (99.95 %) and PEDOT: PSS were purchased from Sigma-Aldrich. $CHCl_3$, acetone, hydrogen peroxide (H_2O_2, 30 wt%) were purchased from Sinopharm Chemical Reagent Co. Ltd. CNT yarn was purchased form Chengdu Organic Chemicals Co. Ltd. All materials were used without further purification.

Synthesis of V_2O_5 nanobelt dispersion. V_2O_5 was synthesized via a modified hydrothermal method. Typically, V_2O_5 (0.364 g) was added to deionized water (30 mL) to form a uniform mixture and then H_2O_2 (5 mL) was added slowly. The resulting solution was stirred for 30 min then transferred into a Teflon-lined stainless-steel autoclave and heated at 220 °C for 96 h. The obtained precipitate was rinsed several times with water and then dispersed in water.

Fabrication of VONS and VONY. V_2O_5 aqueous dispersion was ultrasonicated for 30 s to form a homogeneous dispersion. The dispersion was frozen and then freeze-dried for 2 days. $CHCl_3$ (100 mL) was added to a 500 mL square beaker. V_2O_5 nanobelt dispersion was continuously added on top of the $CHCl_3$ layer to form a water–air–$CHCl_3$ interface. Because of the surface tension, the nanobelts spontaneously assembled and twisted to form yarn. During the continuous addition of V_2O_5 nanobelt dispersion, the yarn which had been formed was collected. Two-step collection process was utilized to avoid rupture in the spinning

process. After fluid-twisting process in three-phase interface, VONY was transferred to a container that full of water.

Simulated calculation of the fluid flow and dynamic pressure of water-$CHCl_3$-air interface. Physical parameters of chloroform are set as 1.48 g/cm^3 density, 0.57 viscosity and 26.5 mN/m, as water phase are 1 g/cm^3 density, 1 viscosity and 72.7 mN/m.

Fabrication of twisted PEDOT: PSS fibers. PEDOT: PSS was injected into acetone through a needle at a flow rate of 3 to 5 mL/h using a microsyringe pump. Original fibers or yarns went through the fluid-twisting process in the $CHCl_3$–water–air interface.

Simulated calculation of twisted fibers by fluid-twisting method. Physical parameters are set as 100 MPa Young's modulus and 1320 kg/m^3 density, similarly to those of graphene oxide in coagulation bath. The load is set according to the movement behavior and dynamic pressure of water–$CHCl_3$–air interface calculated in Fig. 2. With one end constrained (fixed support), graphene fiber shows an apparent helix, demonstrating that the fluid-twisting process can be utilized to twist graphene fibers.

Fabrication of core-sheath semiconductor yarns (CSSY). CNT sheets were drawn from CNT arrays, 18 layers (2-cm width) of which were scrolled into untwisted original yarns. Fibers or yarns (PE, Nylon 6, CNT, etc.) were put into water phase and spin at 180°/s to form a CSSY. Then, further twist was inserted before VONY got dried, until it formed a coiled structure.

Fabrication of coaxial VONY. VONY was wrapped using PDMS with a crosslinking agent and heated in an oven at 80 °C.

Characterization and measurements. Sample morphology was characterized by FESEM (S-4800, Hitachi, Japan). The hierarchical structure was fabricated using an adhesive tape, to

exhibit its layered structures. XRD analysis was carried out on a Rigaku D/max 2550-V X-ray diffractometer using Cu Kα irradiation (λ= 1.5406 Å). The operating voltage and current were kept at 40 kV and 300 mA, respectively. The tensile stress of the aligned yarn was measured on a universal testing machine (Instron Model 5969, Instron, USA). It should be noted that tensile strength was calculated without considering the hollow parts in the cross-sectional area.[1-4] Microscopic images were viewed using an optical microscope (Leica DVM6, Leica, Germany). DSC measurement was done using a differential scanning calorimeter with a 20 ^{o}C/min heating rate (204F1, Netzsch, Germany). SAXS measurement was done using an X-ray scatterometer (SAXSess mc2, Anton Paar, Austria). Electrochemical testing was performed using an electrochemical workstation (VSP-300, Biologic, France). A xenon lamp (XQ500W, Shanghai Lan Sheng Electronics Co., Ltd., China) was used to simulate sunlight for the irradiation testing. Electrical properties of VONY were examined using a multimeter (Keithley 2700, Keithley Instruments, Inc., USA). Actuation of CSSY were recorded by the photos of video camera (EOS D7000, Nikon). The reflectance spectra of CSSY were measured using a fiber-optic UV–vis spectrometer (PG2000-Pro-Ex, Ideaoptics Technology Co., Ltd., China) and spectrometer (CS-820N, Kecheng Instrument Co., Ltd., China). The wavelengths at which the maximum reflectance difference between the redox states was selected to calculate the reflectance contrasts (ΔRT).

Calculation of the aspect ratio of 1D nanomaterials suitable for this preparation method

Taking two parallel nanobelts with a thickness of 50 nm, width of 200 nm, and unknown length as a calculation model, we estimated the adhesion energy of nanobelts using a parallel plate model with the formula:[5]

$$E_1 = \tau lw = \frac{Hlwg_e}{12\pi D^2} \quad (1)$$

where τ is the adhesion energy, g_e is a function based on separation distance, H is the Hamaker constant, and l, and w are the length and width of the nanobelts, respectively. The distance, D between the two nanobelts is estimated to be < 25 nm, from Fig. 1c, and thus τ is estimated to be > 1 μJ/m^2. The interaction energy between nanobelts with their wider surfaces facing each other (E_1) was found to be $l \times w \times 10^{-6}$ J.

The resistances in yarn preparation are mainly surface tension of water–air when breaching the water surface during collection. Thus, the breaching energy (E_2) is given by

$$E_2 = \gamma wh \quad (2)$$

where h is the thickness of the nanobelts. E_2 of the model is estimated to be $3.64 \times 10^{-9} \times w$ J. According to the law of energy conservation and Equation 1 and 2, the nanobelt length needs to be > 3.64 mm to overcome E_2. Therefore, the VONY fabrication process cannot be realized spontaneously when A of the building blocks is < 1.3×10^4.

Applications of VONY in thermistors and photodetectors

The basic semiconductor parameters of the V_2O_5 nanobelts were characterized by ultraviolet photoelectron spectroscopy and ultraviolet–visible (UV–vis) absorption spectroscopy (Fig. S10a and b, Supporting Information). The corresponding band structure of the nanobelts is shown in Fig. S10c, Supporting Information. Electrical property measurements revealed that the conductivity of VONY was ~0.1 S/cm at room temperature, which is similar to that of individual V_2O_5 nanowires (~0.5 S/cm)[6] and higher than that of V_2O_5 bulk films (~10^{-6}–10^{-3} S/cm)[7] because of the ordered crystalline structure of VONY.

Under multiple stimuli, e.g., heat and light, the carrier density of VONY changed, presenting as discrepancies in various electrical signals (Fig. S8a, Supporting Information). The resistance decreased with rising temperature. When repeatedly touched by a finger, VONY showed an electrical signal output with steady resistance variation (Fig. S8c, Supporting Information). Compared with existing semiconductor fibers, VONY could withstand a higher temperature and was suitable for fabricating a high-temperature switch to control a light-emitting diode (LED) (Fig. S8d, Supporting Information). The VONY switch worked by using its resistance decrease with rising temperature to increase the power going to the LED, allowing it to switch on. Thus, VONY expands the working temperature of semiconductor fibers.

For practical applications, a coaxial assembly strategy was designed to prepare transparent polydimethylsiloxane (PDMS)-wrapped VONY. The coaxial yarn was woven into the fabric to construct a textile sensor to detect lesions in human tissues through temperature variation. As shown in Fig. S8e, Supporting Information, a rise in body temperature resulted in different electrical signals, allowing the *in situ* detection of health status. In addition, coaxial VONY is capable of distinguishing the human body from objects (e.g., wood, rubber, glass, polymer, and metal) under ambient conditions. When touched by a finger, which increased the temperature of VONY, the output characteristics of VONY showed pronounced changes. In contrast, the read-out resistance remained unchanged when VONY was touched using other common objects (Fig. S8f, Supporting Information). Position-identification array was fabricated using different combinations of VONY, as illustrated in Fig. S9. Upon pressing at different positions, the array sent a variety of signals to achieve the aim of position identification through multiple electrode channels. When finger touches different positions (*P1-P6* or *C1-C9*), there would be a different signal output at the electrodes (*V1-V6*).

Moreover, the fabric using core-sheath CSSY with nylon fiber core woven into was around the doll's neck, to realize the application of position-identification.

In addition to the temperature sensing application, VONY also demonstrated its utility in photodetectors. V_2O_5 is a direct-bandgap semiconductor with strong optical adsorption in the visible light region, and its conductivity increases drastically upon irradiation with visible light because of the generation of photoexcited electron–hole pairs. The band gap of VONY was determined from its absorption spectrum in Fig. S10a, Supporting Information to be 2.3 eV from the corresponding hv–$(ahv)^2$ spectrum, offering a theoretical basis for blue-light photodetection (460 nm). Fig. S10d of the Supporting Information show the time dependence of the photocurrent change of VONY at a bias of 1 V. Photoresponsivity (R) and detectivity (D^*) can be further expressed by

$$R = \frac{I_{ph}}{PS} \tag{3}$$

$$D^* = \frac{RS^{0.5}}{(2eI_d)^{0.5}} \tag{4}$$

where I_{ph} is the difference between the current under illumination and in the dark, P is the light intensity, S is the effective illuminated area, and I_d is the current in the dark. Using these equations, R and D^* of VONY were found to be 2.66 mA/W and 2.46×10^8 Jones at 20 mW/cm^2. The measured rise and decay times for VONY were 45 and 60 ms, respectively. Compared with other photodetection materials,[8-10] VONY possesses an excellent fibrous structure and photoelectric performance. The stability of the photoresponse of VONY was examined by turning the light on and off for more than 60 cycles, as illustrated in Fig. S10e, Supporting Information. The results demonstrated the stability of VONY in photodetection applications.

Electronic textiles (e-textiles) use a systematic aggregation based on functional fibers or yarns with flexibility and knittability. Coaxial VONY was woven into a fabric (Fig. S10f, Supporting Information), and its corresponding changes in resistance under stimuli of a touch of a finger and blue laser irradiation were observed.

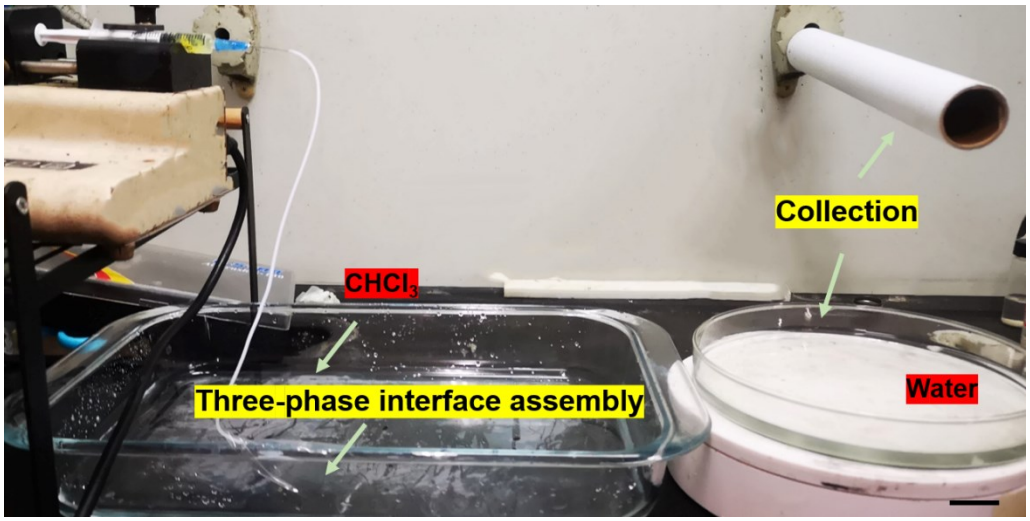

Fig. S1 Digital image of the spinning process of VONY, including the assembly and twist in the three-phase interface, collection in water bath and roller. (Scale bar: 5 cm)

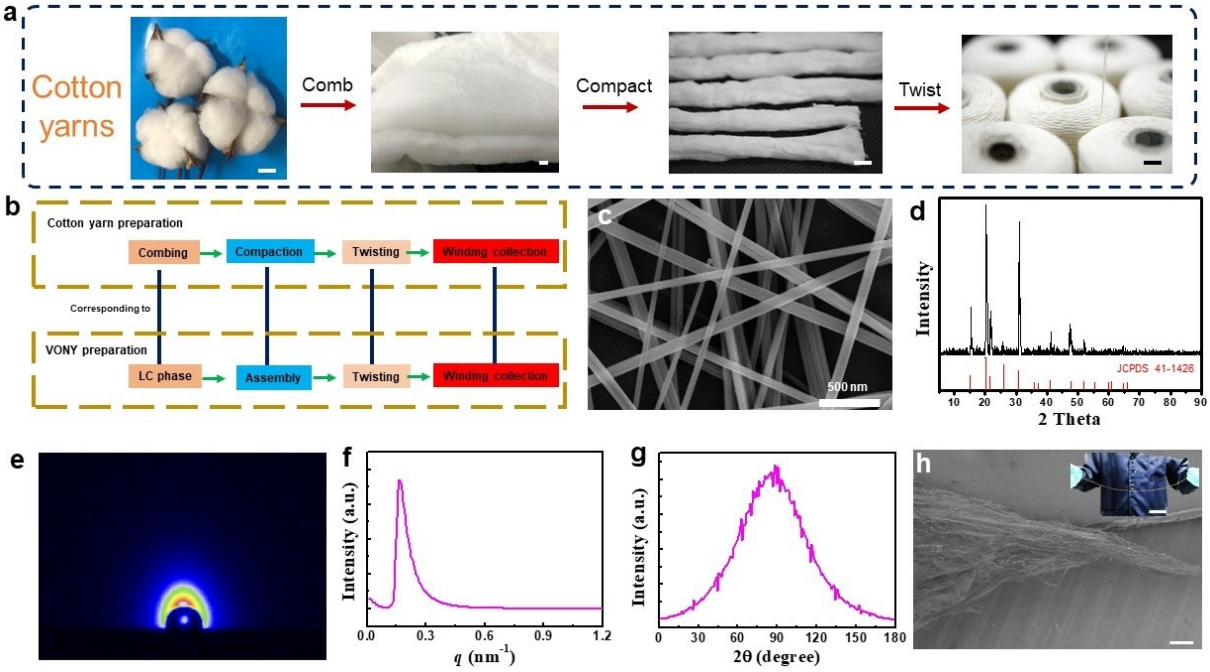

Fig. S2 Fabrication process and characterization of VONY. (a) Digital photograph of the preparation process of cotton yarns including the combing, compaction, and twisting process (scale bars: 1 cm). (b) Schematic diagram of the preparation process of VONY corresponding to the cotton fiber preparation process. (c) FESEM image of V_2O_5 nanobelts. (d) XRD pattern of as- synthesized V_2O_5 nanobelts. (e-g) SAXS measurement of VONY. (h) FESEM image of V_2O_5 nanobelts assembly under twisting process (scale bar: 10 μm). Inset: digital image of free-standing VONY showing good flexibility (scale bar: 10 cm).

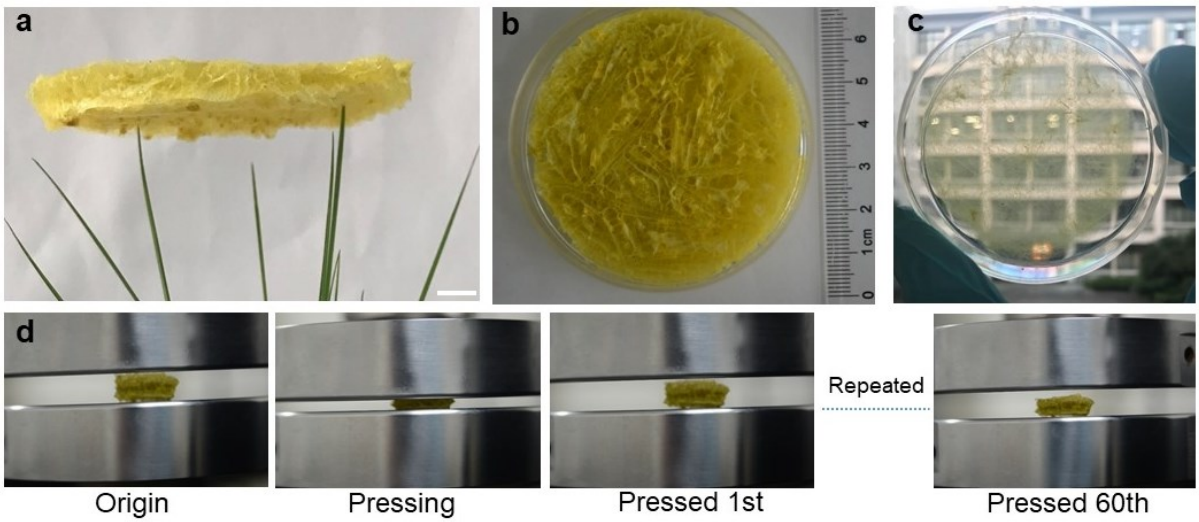

Fig. S3 Digital photos of VONS. (a, b) Digital images of VONS after freeze-drying (scale bar: 1 cm). (c) Digital photograph of ultralight VONS with a density of 0.09 mg/cm^3. (d) Digital photographs of VONS being pressed for 60 times.

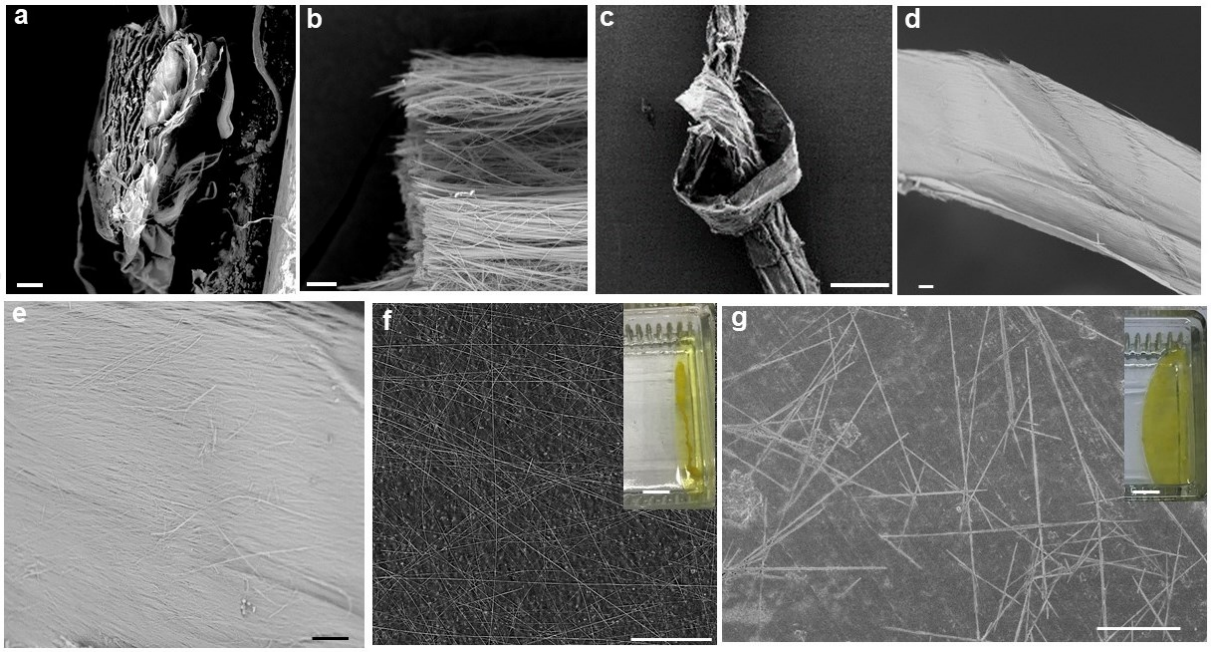

Fig. S4 Structural characterization of VONY. Cross-sectional (a) and high-resolution (b) FESEM images of dried VONY. (c) FESEM image of knotted VONY (scale bar: 500 μm). Low- (d) and high-resolution (e) FESEM images of monolayer VONY peeling through the method similar with that of graphene. FESEM images of V_2O_5 nanobelts after ultrasonic treatment of 2 mins (f) and 30 mins (g) with different aspect ratio. Inset: images of the assembly situations with different *A*.

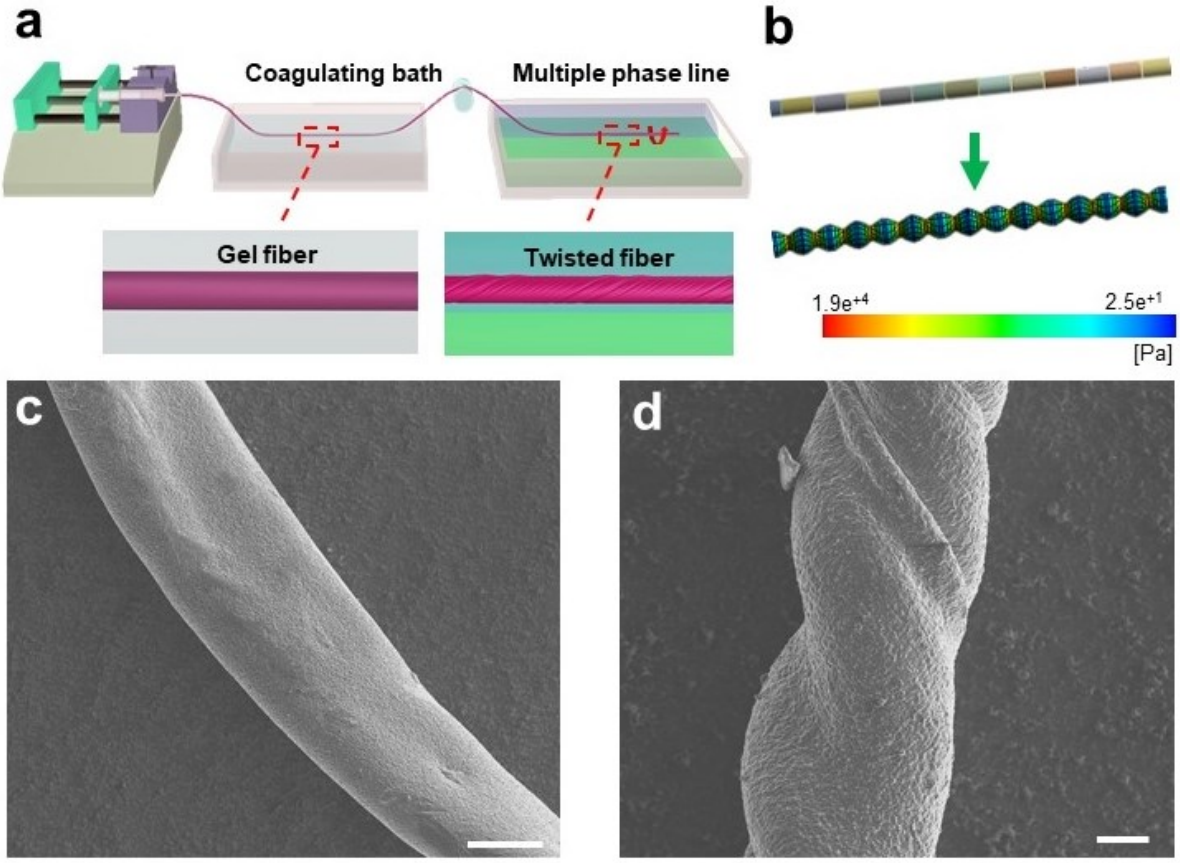

Fig. S5 (a) Schematic of utilization of fluid-twisting to wet-spinning process. (b) Calculated variation of fiber geometry, which physical parameters is set according to those of graphene oxide fibers (scale bar: 1 cm). SEM images of PEDOT:PSS fiber before (c) and after (d) fluid-twisting process.

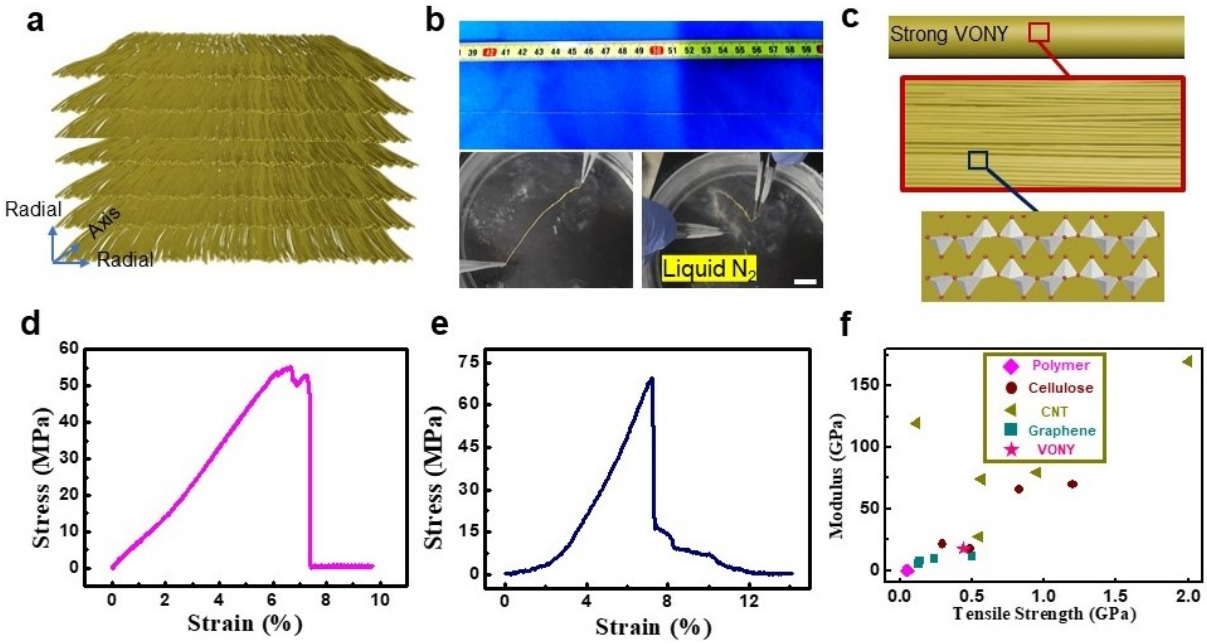

Fig. S6 Physical properties of VONY. (a) Schematic of the hierarchical structure of VONY. (b) Digital image of VONY and bent in liquid nitrogen, showing the flexibility of inorganic VONY under extreme conditions. (c) Schematic diagram of structural characteristics of VONY with an ordered arrangement and covalent bonds in the axial direction. Mechanical test of VONY with graphene oxide (d) and carbon nanotubes (e). (f) The materials data chart of VONY and other nanomaterials fibers.

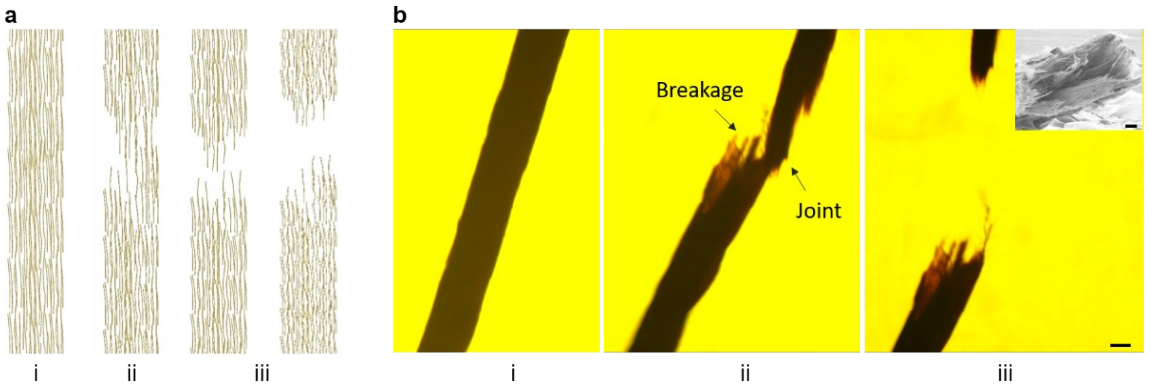

Fig. S7 Schematic diagram (a) and its corresponding optical microscopy image (b) of VONY in the process of tensile measurement (scale bar: 100 μm). Inset: Cross-section SEM image of fractured VONY (scale bar: 100 μm).

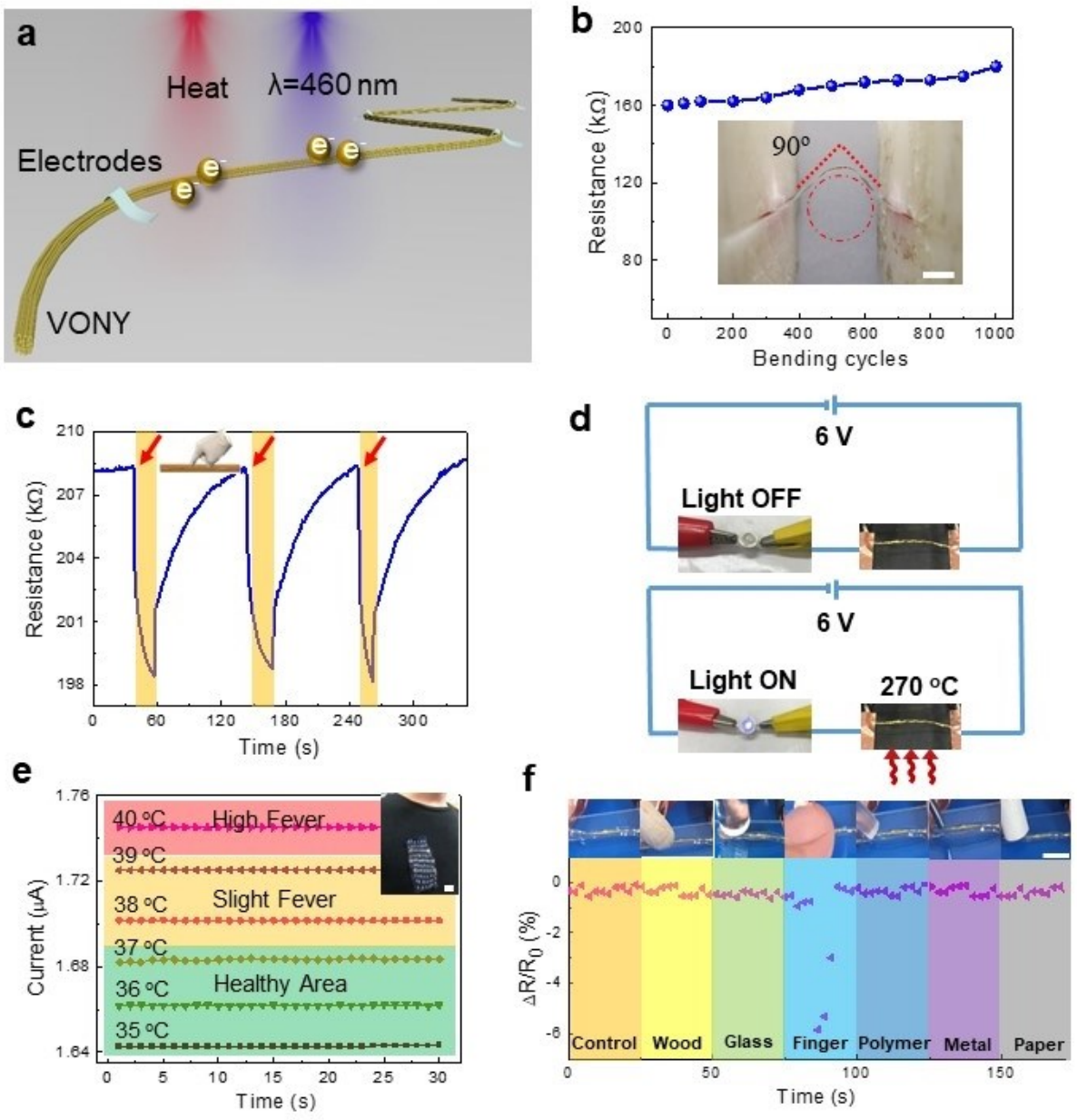

Fig. S8 (a) Schematic diagram of carrier density variation of VONY under stimuli of heat and light of 460 nm wavelength. (b) Resistance variation of VONY during 1000 bending cycles (scale bar: 1 cm). (c) Resistance variation of VONY through repeatedly finger contact. (d) Schematic illustration of a temperature-switch controlling a LED on and off. (e) The textile sensor was stuck to clothes to check body temperature. Inset: Digital photograph of the textile sensor on a human body (scale bar: 1 cm). (f) Photographs and resistance variation showing the different signals of VONY being touched by a human finger and other common objects (scale bar: 5 mm).

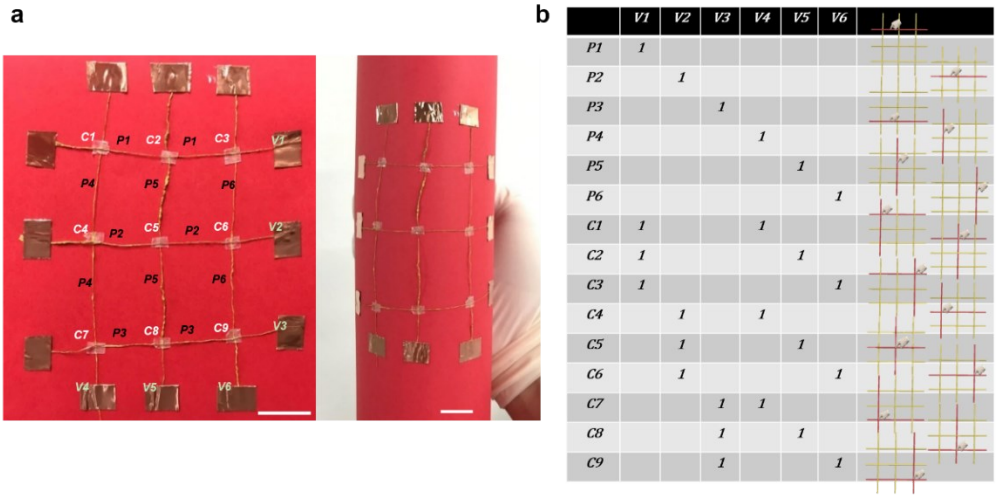

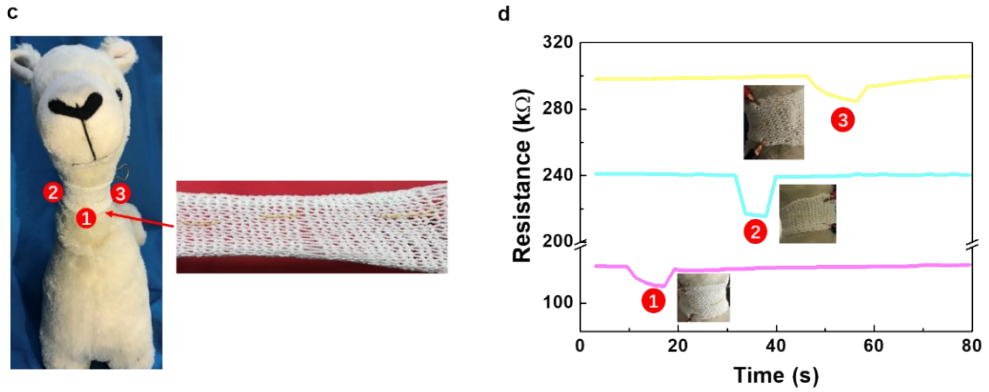

Fig. S9 (a) Digital photographs of VONY arrays for position identification. Scale bar: 1 cm. (b) Various signal output by touching different positions (*P1-P6, C1-C9*), "*1*" indicates a change in VONY resistance. *V* represents measured electrodes for the output signal, *P* and *C* represents the touching of single yarn or cross yarns. (c) Digital photographs of VONY woven into fabric and put around the doll's neck. (d) Different signal output when touching the different positions of the fabric.

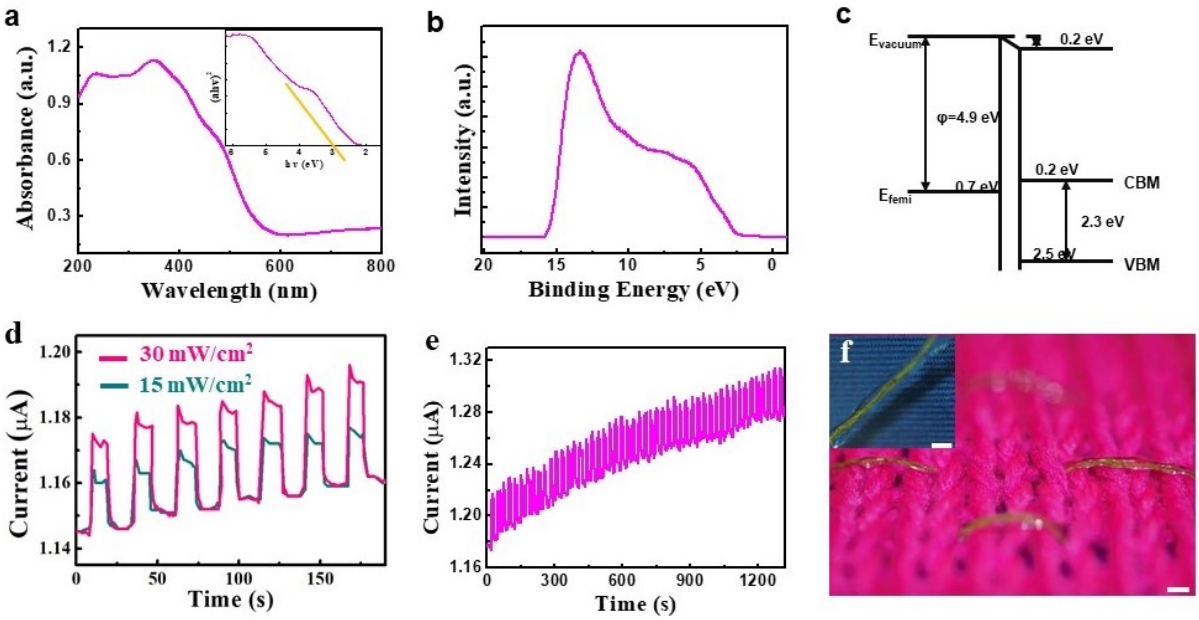

Fig. S10 (a) Ultraviolet (UV)-visible (vis) absorption spectra of VONY. Inset: the corresponding hv-$(ahv)^2$ diagram. (b) Ultraviolet photoelectron spectroscopy (UPS) of VONY. (c) Band structure of VONY. (d) Time dependence of the as-prepared photodetector device with the light intensities of 15 and 30 mW/cm^2 at a voltage of 1 V. (e) Photocurrent versus time curve of the photodetector device with a light density of 30 mW/cm^2 at a voltage of 1 V. (f) Digital photograph of core-sheath VONY woven into a fabric (scale bar: 5 mm). Inset: high-resolution digital photograph of core-sheath VONY (scale bar: 2 mm).

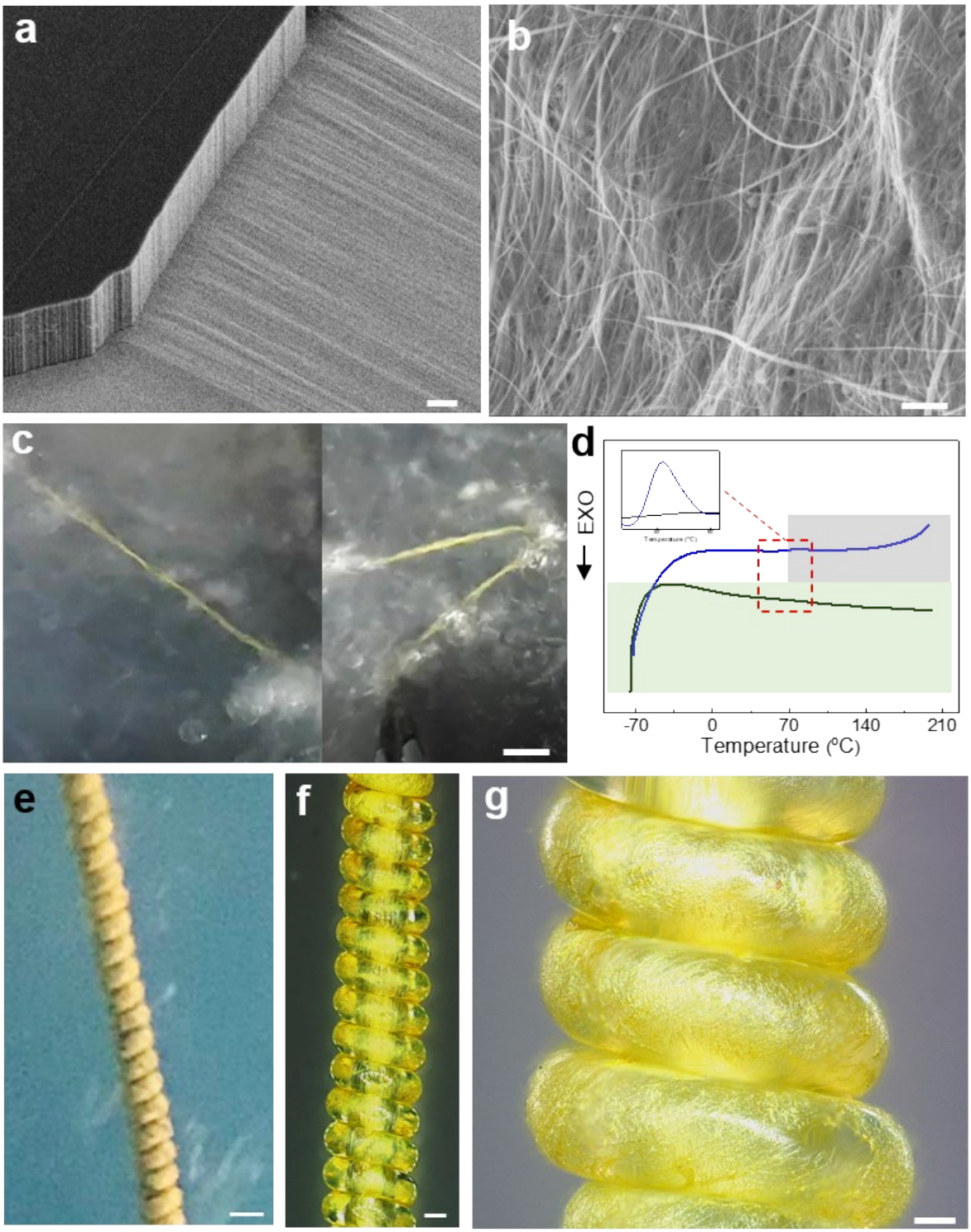

Fig. S11 Structural characterization of CSSY. (a) SEM image of a carbon nanotube sheets in the process of being drawn from a nanotube forest outside the SEM (scale bar: 100 μm). (b) High-resolution SEM image of the sheath of CSSY-CNT (scale bar: 1 μm). (c) Inorganic CSSY-CNT bent in liquid nitrogen. (d) Differential scanning calorimeter (DSC) measurement of polymer (blue line, Nylon 6) and inorganic (black line, CNT) CSSYs. Inset: integrated curve. (e) Digital image of coiled CSSY-CNT (scale bar: 500 μm). (f, g) Digital images of CSSY using PE and Nylon 6 cores (scale bar: 200 μm, 100 μm).

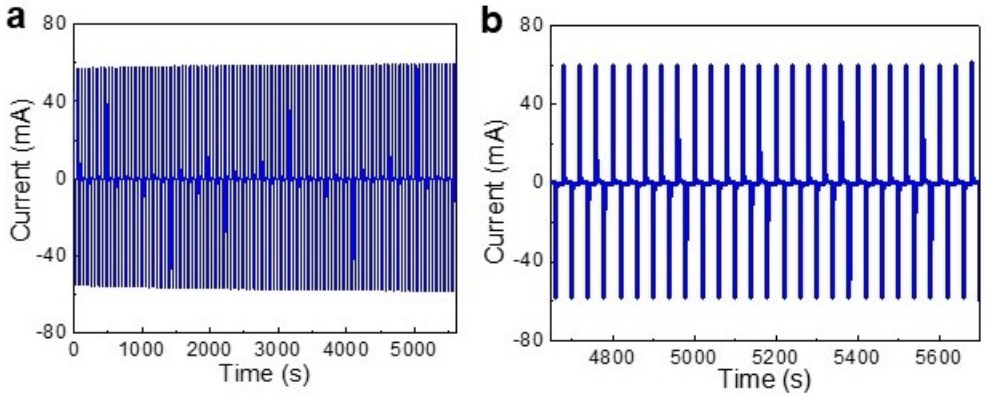

Fig. S12 Dual-responsive performance of CSSY-CNT between -4 V and +4 V. (a) Current response between the colored and bleached states for the dual-responsive yarns and (b) after 150 cycles.

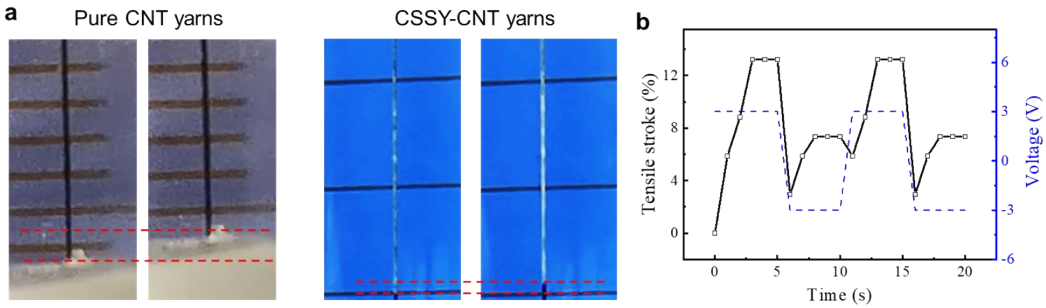

Fig. S13 (a) Digital images of actuation of CNT yarns and CSSY-CNT yarns in an electrolyte under the voltage of 3V, showing the maximum tensile stroke of 10.4% and 4.3 %. (b) The tensile stroke and applied voltage of CNT yarns as a function of time.

Table S1. One dimensional nanomaterials applied for this method.

Materials	Length (um)	Diameter (nm)	Aspect ratio	
Silver nanowires	30	10^2	300	x
Carbon nanotubes	10	5	2000	x
MoO_3 nanobelts	50	100	500	x
$W_{18}O_{49}$ nanowires	8	25	320	x
Bi_2S_3 nanowires	10^2-10^3	200	250-2500	x
Tellurium nanowires	10^2-10^3	4000	25-250	x
V_2O_5 nanobelts	10^3-10^4	100	10^4-10^5	√

Table S2. Ultralight sponges reported.[11-17]

Materials	Density (mg/cm^3)
Silica colloid aerogel	1
Carbon nanotube	0.16

Graphene	0.3
Metal	0.9
Cellular	0.12
Boron nitride	1.4
Fullerene aerogel	1.5
Carbon nanoribbon	4.3
Boehmite sponges	1.2
Vanadium pentoxide	0.09

REFERENCES

1. Y. Bai, R. Zhang, X. Ye, Z. Zhu, H. Xie, B. Shen, D. Cai, B. Liu, C. Zhang, Z. Jia, S. Zhang, X. Li and F. Wei, *Nat. Nanotechnol.*, 2018, **13**, 589.
2. M.-F. Yu, O. Lourie, M. J. Dyer, K. Moloni, T. F. Kelly and R. S. Ruoff, *Science*, 2000, **287**, 637.
3. T. Filleter, R. Bernal, S. Li and H. D. Espinosa, *Adv. Mater.*, 2011, **23**, 2855.
4. M.-F. Yu, B. S. Files, S. Arepalli and R. S. Ruoff, *Phys. Rev. Lett.*, 2000, **84**, 5552.
5. F. W. DelRio, M. P. de Boer, J. A. Knapp, E. David Reedy, P. J. Clews and M. L. Dunn, *Nat. Mater.*, 2005, **4**, 629.
6. J. Muster, G. T. Kim, V. Krstić, J. G. Park, Y. W. Park, S. Roth and M. Burghard, *Adv. Mater.*, 2000, **12**, 420.
7. C. V. Ramana, O. M. Hussain, B. Srinivasulu Naidu, C. Julien and M. Balkanski, *Mater. Sci. Eng. B*, 1998, **52**, 32.
8. Z. Yin, H. Li, H. Li, L. Jiang, Y. Shi, Y. Sun, G. Lu, Q. Zhang, X. Chen and H. Zhang, *ACS Nano*, 2012, **6**, 74.
9. B. Chitara, L. S. Panchakarla, S. B. Krupanidhi and C. N. R. Rao, *Adv. Mater.*, 2011, **23**, 5419.
10. Z. Zheng, L. Gan, H. Li, Y. Ma, Y. Bando, D. Golberg and T. Zhai, *Adv. Funct. Mater.*, 2015, **25**, 5885.
11. W. Lei, V. N. Mochalin, D. Liu, S. Qin, Y. Gogotsi and Y. Chen, *Nat. Commun.*, 2015, **6**, 8849.
12. M. Mecklenburg, A. Schuchardt, Y. K. Mishra, S. Kaps, R. Adelung, A. Lotnyk, L. Kienle and K. Schulte, *Adv. Mater.*, 2012, **24**, 3486.
13. L. Qiu, J. Z. Liu, S. L. Y. Chang, Y. Wu and D. Li, *Nat. Commun.*, 2012, **3**, 1241.
14. S. O. Kucheyev, M. Stadermann, S. J. Shin, J. H. Satcher Jr, S. A. Gammon, S. A. Letts, T. van Buuren and A. V. Hamza, *Adv. Mater.*, 2012, **24**, 776.
15. Y. Si, X. Wang, C. Yan, L. Yang, J. Yu and B. Ding, *Adv. Mater.*, 2016, **28**, 9512.
16. G. Hayase, K. Nonomura, G. Hasegawa, K. Kanamori and K. Nakanishi, *Chem. Mater.*, 2015, **27**, 3.
17. Y. Si, X. Wang, L. Dou, J. Yu and B. Ding, *Sci. Adv.*, 2018, **4**, eaas8925.